https://doi.org/10.1016/j.proci.2018.07.097

Computational realization of multiple flame stabilization modes in DLR strut-injection hydrogen supersonic combustor

Kun Wu[1,2,3], Peng Zhang[2,*], Wei Yao[1,3,*] and Xuejun Fan[1,3]

1. *State Key Laboratory of High Temperature Gas Dynamics, Chinese Academy of Sciences, Beijing, 100190, People's Republic of China*
2. *Department of Mechanical Engineering, the Hong Kong Polytechnic University, Hong Kong*
3. *School of Engineering Sciences, University of Chinese Academy of Sciences, Beijing 100049, People's Republic of China*

Abstract: Inspired by the existence of multiple flame stabilization modes in cavity-assisted supersonic combustor, multiple flame stabilization modes of DLR hydrogen-fueled strut injection supersonic combustor were numerically realized and analyzed for a wide ranges of inflow stagnation temperature from 607 to 2141 K and overall equivalence ratio from 0.022 to 0.110. Finite-rate chemistry large eddy simulation with detailed hydrogen mechanism was employed to capture unsteady flow characteristics and the effects of chemical kinetics. Two typical flame stabilization modes were identified and presented in a regime nomogram, which shows the dominant influence of the stagnation temperature and the secondary influence of overall equivalence ratio. At relatively low stagnation temperatures, the flame is stabilized in an "attached flame" mode, which requires a low-speed recirculation zone behind the strut for radical production and a high-speed intense combustion zone for heat release. At relatively high stagnation temperatures, the flame is stabilized in a "lifted flame" mode, in which the effect of the low-speed recirculation zone is negligible, rendering most reactions take place in supersonic flow. At intermediate stagnation temperatures, blow-out was always observed and flame cannot be stabilized in the combustor even with initially forced ignition.

Keywords: Supersonic combustion; Flame stabilization mode; DLR Strut injection scheme; Stagnation Temperature; Overall equivalence ratio.

* Corresponding Author: pengzhang.zhang@polyu.edu.hk (P. Zhang) and yaowei@imech.ac.cn (W. Yao)

1. Introduction

Although scramjets have shown their great potential in air-breathing propulsion at high flight Mach numbers [1], many technical problems remain unsolved. One of the problems is the flame stabilization in scramjet with moderate flight Mach numbers of 3~4, where the intake flow temperature is insufficiently high for subsequent auto-ignition after initial forced ignition and therefore additional flame-holding device is required. Wall injection [2], ramp [3], cavity [4] and strut [5] are widely-used flame-holding devices to generate low-speed flow regions where the local Damköhler numbers are effectively increased to enforce flame stabilization.

The flame stabilization mode of cavity flame holder in a dual-mode combustor fueled by both hydrogen and hydrogen/ethylene mixture was experimentally studied by Micak and Driscoll [6]. They found that the flame is stabilized either in the cavity shear layer at relatively low inflow stagnation temperature (T_0) or in the fuel jet-wake at higher T_0, and that combustion oscillates between two modes for intermediate T_0. By employing CH* chemiluminescence to diagnose an ethylene-fueled supersonic combustor with T_0 between 1200 K to 1800 K, Yuan et al. [7] recently identified three flame stabilization modes: (I) weak combustion inside the cavity or in the cavity shear layer, (II) combustion in the jet-wake, and (III) combustion oscillation between modes I and II.

Despite that these experiments are evidently different in combustor geometry, fuel injection location and fuel reactivity, the flame stabilization modes seem to be unified and the underlying physics can be understood as follows. At relatively low T_0, the chemical reactions are extremely slow in the main stream and the cavity facilitates combustion by prolonging the flow residence and fuel/oxidizer mixing times, rendering a local region of large Damköhler numbers. The cavity plays an indispensable role in providing hot spots and radicals so that the reaction zone can reside either in cavity or in the cavity shear layer (mode I).

Increasing T_0, the chemical reaction rates are increased exponentially to mitigate the reliance of the stabilized combustion on the low-speed cavity flow. As a result, reactants can be mixed and auto-ignited over a certain streamwise distance in the fuel jet-wake (mode II). Yuan et al. [8] hypothesized that the formation of aerodynamic throat near the fuel injection is germane to the observation of mode III for intermediate T_0.

Is the occurrence of these flame stabilization modes unique for cavity-based supersonic combustor? Can we observe them in strut-based supersonic combustor by varying T_0 or fuel injection? Bearing these questions in mind, we noted that a strut-injection hydrogen supersonic combustor was established by Institute of Chemical Propulsion of the German Aerospace Center (referrer to DLR combustor [9], hereinafter). The DLR experiments have been widely used for validating various numerical methods and codes, but only a few studies concern about its flame stabilization mode. Huang et al. [10] reported in their LES study that the wall-reflected oblique shock induces combustion in the subsonic bubble after the strut. Gong et al. [11] regarded the oscillation of the recirculation zones as the dominating mechanism for flame stabilization. Recently, Wu et al. [12] proposed a three-stage flame stabilization mechanism based on the analysis of generation, transportation and consumption of radicals. Regardless of the different explanations, the DLR combustion is agreed to be categorized to mode I in which the flame is attached to the fuel injection strut. This is because the relatively low T_0 hinders auto-ignition, and the combustion behind the strut, which plays the same role as cavity in creating a low-speed recirculation zone, is necessary to sustain combustion in the downstream.

Because of the fixed T_0 (607 K) and fuel injection, the DLR supersonic combustion experiment does not show any evidence for mode II or III. Qin et al. [13] carried out a LES study on the DLR combustor with three different T_0 of 460K, 568 K and 960 K, but with fixed Mach number and global equivalence ratio. They found that, the stabilized flames at

460 K and 568 K are similar to modes I but the combustion eventually dies out at 960K after initial forced ignition. Therefore, the problems still remain unsolved that whether mode II and III can exist for the DLR combustor and that what is the underlying physics in terms of flow-chemistry interaction. The present study aims to computationally reproduce and characterize main features of these different flame stabilization modes in strut-injection DLR combustor.

2. Computational Specifications

2.1 Numerical methods and physical models

The numerical methods and physical models adopted by the present study have been expatiated in great detail and sufficiently validated in [12]. As a brief summary, the spatially filtered equations for three-dimensional, compressible, multicomponent, reacting flow are solved. The ideal gas mixture is assumed to be linear viscous fluid abiding Fourier heat conduction and Fickian diffusion; the viscosity is calculated by Sutherland's law; thermal conductivities and mass diffusivities are obtained from viscosity by assuming constant Prandtl number ($Pr = 0.7$) and Schmidt number ($Sc = 0.7$). The subgrid turbulence terms are closed by employing the one-equation kinetic energy model [14]. Turbulent Prandtl number, Pr_{t}, and Schmidt number, Sc_{t}, are set to 0.72 and 0.9, respectively. The filtered reaction rates are modeled using the partially stirred reactor (PaSR) model [15], which and its variation [16] have been extensively used in the studies of self-ignition [17] and supersonic combustion [18].

A density-based flow solver, astroFoam, which was developed based on the OpenFoam platform, was adopted in the study. The convective fluxes at faces are constructed using a second-order TVD (Total Variation Diminishing) scheme. The time-integration is marched by the second-order Crank-Nicholson scheme [19]. This code has been extensively validated for non-reactive highly underexpanded jet [20] and supersonic combustion [21].

2.2 Computational setups

The DLR combustor [9] is schematized in Fig. 1. Coordinates in both x and y directions are normalized to $\hat{x}$ and $\hat{y}$ using combustor's characteristic length L and height H. Ma=2.0 vitiated air was supplied through a rectangular-shaped entrance of 50 mm in height and 40 mm in width. The combustor upper wall diverges slightly by 3° from $\hat{x} = -0.039$ to compensate the growing boundary layer. Hydrogen was sonically injected from an array of 15 evenly-spaced injectors on the base of a wedge-shape strut. The strut is 32 mm in length and 6° in half divergence angle and installed along the combustor center line. The fuel orifices at $\hat{x} = 0$ are 1.0 mm in diameter and their adjacent distance is 2.4 mm in the z-direction.

In the DLR experiment, the air stagnation pressure and temperature are 0.78 MPa and 607 K. The vitiated air was composed by oxygen of 23.2%, nitrogen of 73.6% and vapor water of 3.2% in mass. The fuel stagnation pressure and temperature are 0.189 MPa and 288 K; the overall equivalence ratio is $\phi_{overall} = 0.034$. For the present computational study, the inflow stagnation temperature (T_0) varies over a wide range from 607 K to 2141 K and $\phi_{overall}$ varies significantly from 0.022 to 0.110. To facilitate the following discussion, velocity, temperature and heat release rate are presented in dimensionless form of $\hat{u}_i = u_i/U_\infty^{air}$, $\hat{T} = T/T_\infty^{air}$, $d\hat{Q} = dQ/C_pT$, and $\hat{T}_0 = T_0/T_0^{exp}$.

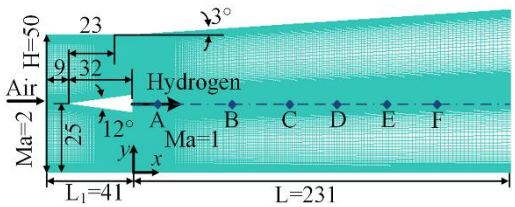

Fig. 1. Schematic of the DLR combustor (unit in mm).

The present work adopts the 2D computational model proposed by Wu et al. [12]. In the 2D model shown in the Support Materials (Fig. S1), the fuel orifice is replaced by a 2D slot-like injector with a periodic injection scheme to keep $\phi_{overall}$ the same as in the experiment and meanwhile retains the local flow structures in the vicinity of the strut. The applicability

of the 2D model in capturing the spatial distributions of pressure, velocity, and temperature was fully validated, and its uncertainty in resolving the near-field turbulent wake structures was also recognized [12]. It should be emphasized that the 2D model can remarkably reduce the computational cost, particularly when the computation is integrated with the Burke et al.'s [22] detailed hydrogen oxidation mechanism consisting of 9 species and 19 reactions, to enable the systematic study of flame stabilization and the result analysis from the perspective of chemical kinetics.

Block-structured hexahedral grids were used with clustering applied at the strut shear layer and wake region. The average and maximum of the grid resolution in the mixing region are 0.08 mm and 0.15 mm, respectively. They are smaller than 0.25 mm (in average) in the hybrid LES/RANS study of Potturi and Edwards [23] and 1.0 mm (in average) in the LES study of Génin and Menon [24]. The comprehensive grid convergence study based on three sets of grid (0.19, 0.27 and 0.52 Million) has been presented in [12] and further study in the Supporting Materials (Fig. S2-S3). Dirichlet boundary conditions are used for all variables at the air and fuel inlet except for velocity. The velocity profile at the inflows is specified as a superposition of their mean values and sinusoidal perturbation with 5% of their amplitude of the mean values. At the combustor outlet, all variables are extrapolated from the interior. At the combustor and strut walls, no-slip boundary condition is used for velocity while zero gradient conditions are used for all other variables. The physical time step is set to 3.5×10^{-9} s which corresponds to a maximum Courant-Friedrich-Lewy number of 0.4. The simulations were run for about 14 flow-through times ($t_f = L/U_\infty \approx 3 \times 10^{-4}$ s), where $7t_f$ was used to ensure statistical steady state while the remainder to collect statistical data.

3. Results and Discussion

3.1 Numerical validation

The present 2D model has been validated in [12] against the DLR experiment [9], and compared with Potturi et al.'s [23] simulation results. To further examine its uncertainty in predicting turbulent flow, the LES results of Fureby et al. [25] on the full-scale DLR combustor including all fifteen fuel injectors are presented in Fig. 2 for comparison. The streamwise locations are annotated in Fig.1 where $\hat{x}_A = 0.048$, $\hat{x}_B = 0.251$, $\hat{x}_C = 0.390$, $\hat{x}_D = 0.498$, $\hat{x}_E = 0.606$ and $\hat{x}_F = 0.719$.

The DLR experiment reported the measurement of streamwise velocity at locations A, B and E, as shown in Fig. 2(a)-(c). At location A, the 2D model overpredicts the streamwise velocity, probably attributable to its uncertainty in resolving the three-dimensional flow structure in the near field around the strut rear. Qualitative discrepancies can be found between Fureby et al.'s prediction and the experimental data. At location B, the predicted velocity profile, albeit narrow in width, agrees well with the trend of the experimental data. At location E, the present result shows very good agreement with the experimental data, but Fureby et al.'s results however show an opposite trend. The comparison with 3D simulation has been elaborated in Ref [12]. Although the present 2D model may result in the single temperature peak due to the relative deficiency in fully capturing the 3D flow characteristics in the vicinity of the strut, it produces good predictions in all the downstream locations.

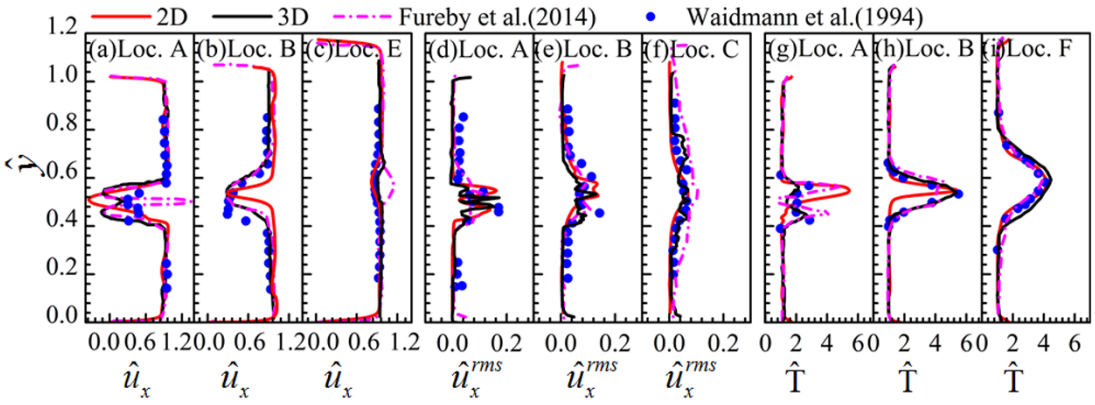

Fig. 2. Time-averaged profiles of streamwise velocity, streamsise velocity fluctuation, and temperature at streamwise locations.

The experimental fluctuation velocity profiles are available at locations A, B and C, as shown in Fig. 2(d)-(f). The present results show very good agreement with experimental data, indicating that the 2D model can well capture the unsteadiness of the streamwise flow that dominates the DLR flow. Fureby et al.'s results slightly overshoot the experimental data at location C. Fig. 2(g)-(i) show the time-averaged temperature profiles at location A, B, and F. It can be seen that the both simulated temperature profiles do not reproduce the two temperature peaks at location A, while they achieve satisfactory good agreement at the downstream locations B and F. Due to the lack of experimental data at higher T_0, the present 2D model was further validated against 3D simulation for T_0=2141 K, the highest T_0 considered in the study. These results are shown in the Supporting Materials (Fig. S4-S5) and further validate the 2D model at high T_0.

3.2 Attached flame stabilization mode

A representative (original experimental) case of the attached flame stabilization mode is shown in Fig. 3, where $T_0 = 607$ K and $\phi_{overall} = 0.034$. As has been thoroughly analyzed in [12], the entire combustion process can be divided into three stages along the streamwise direction, such as the induction stage where ignition occurs and active radicals are produced, the transitional stage through which radicals are advected to the downstream, and the intense combustion stage where most heat release occurs. From the mass fraction of OH radicals, as shown in Fig. 3(a), the three-stage combustion stabilization mode can be clearly observed, indicating the radical production, transportation and consumption are essential in attached flame stabilization mode. Moreover, the time-averaged result, as seen in Fig. S6 in the Supporting Materials, also shows similar characteristics and further substantiates the assertion of the three-staged flame stabilization mode.

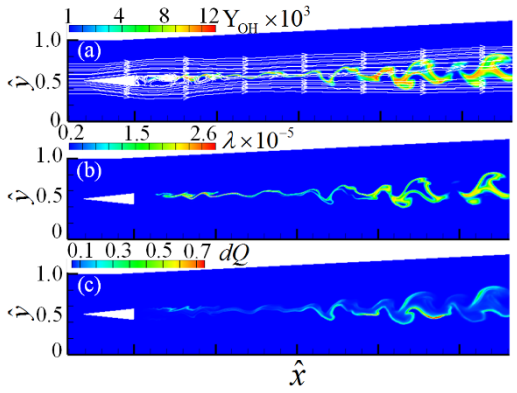

Fig. 3. Representative case of attached flame stabilization mode with $T_0 = 607$ K and $\phi_{overall} = 0.034$: (a) instantaneous Y_{OH}, (b) instantaneous mixture reactivity and (c) instantaneous heat release rate.

By comparing hydrogen oxidation mechanisms at various different levels of reduction, the controlling reaction steps were identified by Wu et al. [12] to be the two chain branching reactions (R1) $H+O_2 \rightarrow O+OH$ and (R2) $O+H_2 \rightarrow H+OH$, both of which produce OH radicals, and (R3) $H_2+OH \rightarrow H+H_2O$, which consumes OH radicals and releases heat. To quantitatively measure the competition among these reaction steps, we adopted the mixture reactivity, λ, defined by Boivin et al. [26] as $\lambda = 2k_1c_{O_2}\left[(1+2B)^{1/2}-1\right]/B$, where $B = 4k_1c_{O_2}(k_1c_{O_2}+k_2c_{H_2}+k_3c_{H_2})/k_2k_3c_{H_2}^2$. k_1, k_2 and k_3 are the rate constants of R1, R2 and R3, and c the molar concentration of species. According to the definition, the mixture reactivity index λ is inversely proportional to the auto-ignition delay time under homogeneous conditions. Consequently, a large value of λ means that reaction R1 and R2 control the reactivity of the mixture and facilitate ignition. For small λ, reaction R3 dominantly consumes OH radicals and therefore retards ignition.

Figure 4 shows λ, Y_{OH}, and $d\hat{Q}$ in a Mach number space. The evident concentration of λ and Y_{OH} in the subsonic regime reemphasizes the important role of the low-speed recirculation zone behind the strut in producing active radicals. In contrast, $d\hat{Q}$ is distributed over the whole Mach number range, indicating that both the recirculation zone and the downstream intense combustion zone are responsible for the heat release.

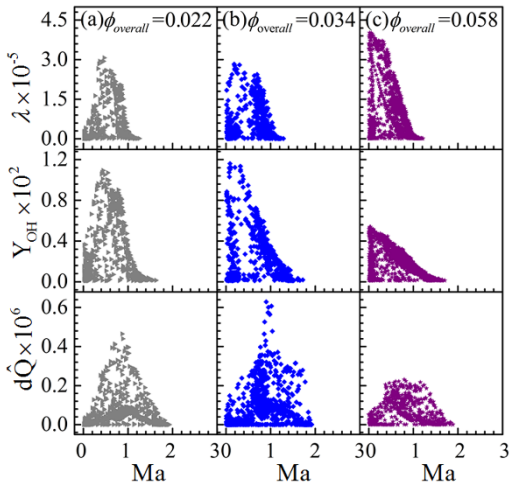

Fig. 4. Distribution of λ, Y_{OH} and $d\hat{Q}$ in Mach number space with $T_0 = 607$ K and $\phi_{overall}$ equals to (a) 0.022, (b) 0.034, and (c) 0.058.

With decreasing $\phi_{overall}$ to 0.022, as shown in Fig. 4(a), peak values of λ and Y_{OH} tend to shift to higher subsonic regime. This can be understood that, because of the reduced total heat release at the smaller $\phi_{overall}$, the thermal expansion of the reaction zone becomes smaller as shown in Fig. S7(a)-S9(a) in the Supporting Material. Therefore, the influence of the reaction zone on the main stream is reduced. With increasing $\phi_{overall}$ to 0.058, more heat release and the wider reaction zone can be seen, as shown in Fig. S7(c)-S9(c) in the Support Material. This in turn decelerates the main stream so that the combustion in the strut wake is intensified. This tendency can be seen in Fig. 4(c) where the reaction zones show subsonic-shifting and the peak values of λ and Y_{OH} move to smaller Ma. Regardless of these changes, the main feature of the attached flame stabilization mode is retained. Furthermore, the backpressure caused by the increased heat release in the present case is insufficient to alter the combustor inflow condition. Therefore, the combustor unstart observed by Zhang et al. [27] in cavity flame-holding supersonic combustor by increasing fuel injection was not observed in the present study.

3.3 Lifted flame stabilization mode

Fig. 5 shows the case with $T_0 = 1784$ K and $\phi_{overall} = 0.058$. The low-speed recirculation zone indicated by the converging streamlines behind the strut is suppressed by the main flow to a very small region, where Y_{OH} is negligibly small. The distribution of λ is similar to that of Y_{OH} and again indicates that R1-R3 are all suppressed in the strut wake flow. The little reliance of the flame stabilization on the local recirculation zone and the far downstream location of the lifted flame suggest that the present stabilization model resembles the fuel jet wake in the cavity-based supersonic combustion experiment [6]. Furthermore, the time-averaged result, as shown in Fig. S10 in the Supporting Materials, also resembles similar lifted flame stabilization characteristics. It is noted that the present fuel injection is made on the base of the strut so that the jet wake is in the downstream of the strut. In the cavity-based supersonic combustor [7, 8], a cross-flow of fuel was injected to the upstream of the cavity and the jet wave is above the cavity.

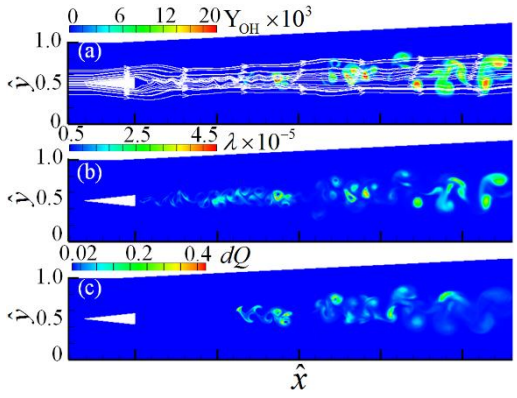

Fig. 5. Lifted flame stabilization mode with $T_0 = 1784$ K and $\phi_{overall} = 0.058$: (a) instantaneous Y_{OH}, (b) instantaneous mixture reactivity and (c) instantaneous heat release rate.

To further reveal the difference between two flame stabilization modes, plots of Y_{OH}, λ, $d\hat{Q}$ in the mixture fraction space are presented in Fig. 6. The mixture fraction (denoted by Z) refers to the conventional definition [28] as $Z = (\upsilon Y_F - Y_{O2} + Y_{O2,2})/(\upsilon Y_{F,1} + Y_{O2,2})$ in which υ is the stoichiometric oxygen-to-fuel mass ratio. In the strut shear layer and wake flow near the fuel injection, the mixture ranges from fuel rich to nearly stoichiometric rendering $Z \geq Z_{st}$. As the result of the mixing between the fuel jet and main air flow, Z

gradually decreases in the downstream. For the attached flame mode at $T_0 = 607$ K, most OH appears around Z_{st}, implying that it forms in the recirculation zone with long flow residence time for mixing. Similar trend can be found for λ since it represents the competition among reaction R1-R3 for OH radicals. For the lifted flame mode at $T_0 = 1784$ K, most OH appears at $Z<Z_{st}$, implying that it is not formed in the "fuel-rich" recirculation zone but in the "fuel-lean" far downstream.

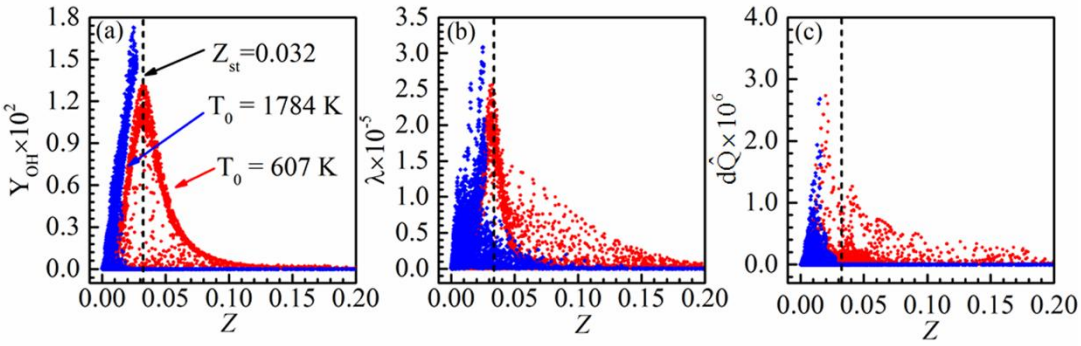

Fig. 6. Scatter points' distribution in mixture fraction space for attached flame stabilization mode at $T_0 = 607$ K and lifted flame stabilization mode at $T_0 = 1784$ K.

Fig. 7 shows λ, Y_{OH}, and $d\hat{Q}$ in Mach number space for various T_0. Regarding Y_{OH} and $d\hat{Q}$, the most prominent feature of the lifted flame mode is the transition of the primary combustion zone to the supersonic regime, compared with that in Fig. 4. It is also found that the lifted flame at $T_0 = 1696$ K moves to farther downstream and significantly decreased radical formation and heat release occur in the supersonic regime, indicating the increasing tendency of the flame blow-out with decreasing T_0.

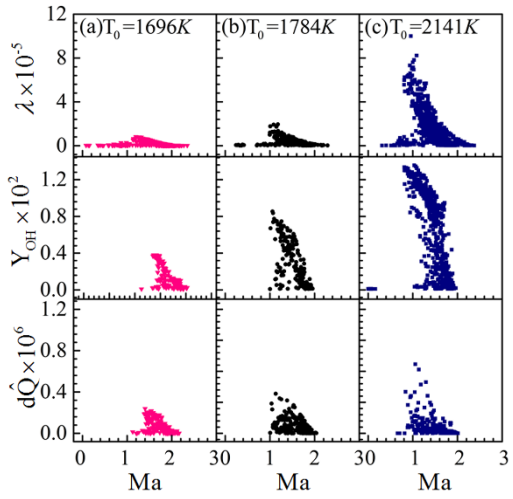

Fig. 7. Distribution of λ, Y_{OH} and $\mathrm{d}\hat{\mathrm{Q}}$ in Mach number space with (a) $T_0 = 1696$ K, (b) $T_0 = 1784$ K, and (c) $T_0 = 2141$ K.

It is rather interesting to investigate the flame lift-off distance as an indicator of flame blowout trend. By following the definition introduced by Micka and Driscoll [6], an iso-line characterizing the reaction zone border was defined in instantaneous OH contour with prescribed threshold value, i.e., $Y_{OH}(Threshold) = 10^{-5}$. The most upstream axial locations of a series of temporal snapshots were calculated then averaged to get the final statistical result as shown in Fig. 8. To verify that the flame lift-off distance is insensitive to the threshold, two different thresholds by an order of magnitude were used and both show the consistent tendency as follows. In the present problem with a fixed Mach number, higher T_0 means higher static temperature T and speed of sound ($c \sim \sqrt{T}$), which tends to push the flame further downstream. In the meantime, the increased temperature will exponentially increase chemical reaction rates [$\sim \exp(-E_a/RT)$], rendering the intense combustion in higher velocity flow possible. This explains the lift-off distance in the lifted flame stabilization mode decreases with T_0.

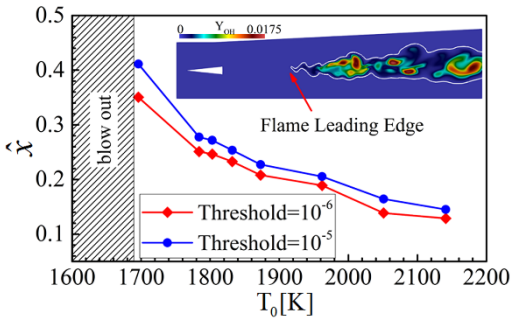

Fig. 8. Dependence of the flame lifted length on T_0 for the strut-based lifted flame stabilization mode.

3.4 Regime nomogram for strut-based flame stabilization

To systematically quantify the influence of T_0 and $\phi_{overall}$ on the flame stabilization, we studied 21 cases with T_0 varies from 607 K to 2141 K and $\phi_{overall}$ from 0.022 to 0.110. Details of all the cases are listed in Table S2-S3 in the Supporting Material. It is noted that the variation of T_0 with the fixed Mach number slightly changes the air flow rate and thus the overall equivalence ratio by 13% in maximum, which does not cause qualitative difference to the flame stabilization modes, as has been substantiated above.

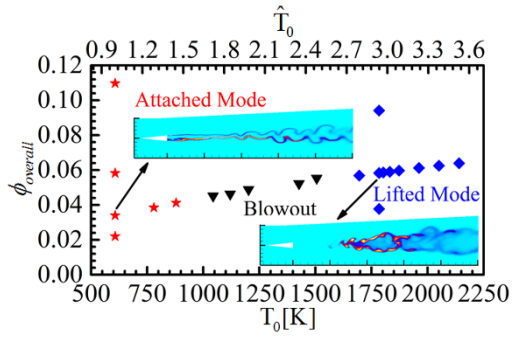

Fig. 9. Regime nomogram for the DLR flame stabilization.

The identified flame stabilization modes are depicted in Fig. 9 as a regime nomogram in the $T_0 - \phi_{overall}$ space. Under relatively low T_0, the flame in the DLR combustor stabilizes in attached mode while $T_0 \geq 1696$ K the flame can again be stabilized however in another distinct mode. It is also seen that the variation of $\phi_{overall}$ in the range concerned does not cause transition between attached and lifted flame stabilization modes, indicating that overall

equivalence ratio is a secondary factor in determining flame stabilization mode in the DLR combustor. The influence of $\phi_{overall}$ on the combustion characteristics is shown in Fig. S11-S14 in Supporting Material.

In the intermediate temperature range of $1044 < T_0 < 1696$ K, the flame cannot be stabilized even being forced ignited initially. This has been confirmed by our repeated simulation runs by using different initial conditions and ignition methods. In fact, at the fixed inflow Mach number, the inflow velocity increases with T_0 and causes more heat loss from the combustion zone to the main air flow, therefore tending to destabilize the flame. This can be used to explain why combustion oscillation, which was hypothesized to occur in this temperature range, was not observed in the present simulation. As elaborated in the introduction, the formation of aerodynamic throat is essential for oscillation flame stabilization mode but the combustion in DLR configuration is unable to provide sufficient heat release to thermally chock the combustor. Therefore, the oscillation between the two modes could not be realized in the present study. A possible solution to the problem is to modify the geometry of the DLR combustor to increase the possibility of thermal chocking. This hypothesis merits future investigations.

4. Concluding Remarks

In the present study, flame stabilization modes in a hydrogen-fueled strut injection DLR supersonic combustor were systematically investigated employing finite-rate chemistry large-eddy simulation with detailed hydrogen mechanism of Burke et al. [22] . Two different flame stabilization modes were identified by multiple metrics such as flow field visualization, radical evolution, and heat release, in both Mach number and mixture fraction spaces.

For the attached flame stabilization mode occurring at relatively low T_0 (607 to 879 K), the entire combustion process can be divided into three stages, such as the induction stage where ignition occurs and active radicals are produced, the transitional stage through which radicals are advected to the downstream, and the intense combustion stage where most heat release occurs. The low-speed recirculation zone behind the strut is indispensable to the combustion stabilization by producing active radicals.

For the lifted flame stabilization mode occurring at relatively high T_0 (1696 to 2141 K), a lifted flame is manifest and the effect of the low-speed recirculation zone behind the strut becomes negligible. Furthermore, the flame lifted distance deceases with increasing T_0 because the exponentially increased reaction rates shorten the distance between the fuel injection and the autoignition. In contrast to that the main combustion zones of the attached flame mode resides in subsonic regions, the main combustion zone in the lifted flame mode is in the supersonic region.

The present parametric study shows that significant variation in the overall equivalence does not cause the change of stabilization mode. In the intermediate range of T_0 (1044 to 1506 K), the hypothesized combustion oscillation was not observed and the initially forced ignition always results in eventual blowout. The existence of combustion oscillation mode in the DLR supersonic combustor remains an unsolved problem.

Acknowledgements

The work at Chinese Academy of Sciences was supported by Training Program of the Major Research Plan of the National Natural Science Foundation of China (Grant No. 91641110) and National Natural Science Foundation of China (Grant No. 11502270). The

work at the Hong Kong Polytechnic University was supported partly by RGC/GRF (PolyU 152217/14E, PolyU 152651/16E) and partly by NSFC (No. 91641105).

References

[1] J.J. Bertin, R.M. Cummings, Prog. Aerosp. Sci., 39 (2003) 511-536.

[2] W. Xianyu, L. Xiaoshan, D. Meng, L. Weidong, W. Zhenguo, Chin. J. Aeronaut., 20 (2007) 488-494.

[3] J.M. Donohue, J.C. McDaniel, H. Haj-Hariri, AIAA J., 32 (1994) 1860-1867.

[4] F.W. Barnes, C. Segal, Prog. Aerosp. Sci., 76 (2015) 24-41.

[5] K.Y. Hsu, C.D. Carter, M.R. Gruber, T. Barhorst, S. Smith, J. Propul. Power, 26 (2010) 1237-1246.

[6] D.J. Micka, J.F. Driscoll, Proc. Combust. Inst., 32 (2009) 2397-2404.

[7] Y. Yuan, T. Zhang, W. Yao, X. Fan, P. Zhang, Proc. Combust. Inst., 36 (2017) 2919-2925.

[8] Y. Yuan, T. Zhang, W. Yao, X. Fan, J. Propul. Power, 31 (2015) 1524-1531.

[9] W. Waidmann, F. Alff, M. Böhm, U. Brummund, W. Clauß, M. Oschwald, Space Technol., 15 (1994) 421-429.

[10] Z.-w. Huang, G.-q. He, F. Qin, X.-g. Wei, Int. J. Hydrogen Energy, 40 (2015) 9815-9824.

[11] C. Gong, M. Jangi, X.-S. Bai, J.-H. Liang, M.-B. Sun, Int. J. Hydrogen Energy, 42 (2017) 1264-1275.

[12] K. Wu, P. Zhang, W. Yao, X. Fan, Combust. Sci. Technol., 189 (2017) 2154-2179.

[13] F. Qin, Z.-w. Huang, G.-q. He, S. Wang, X.-g. Wei, B. Liu, Int. J. Hydrogen Energy, 42 (2017) 21360-21370.

[14] A. Yoshizawa, Phys. Fluids, 29 (1986) 2152-2164.

[15] A. Karlsson, Modeling Auto-ignition, Flame Propagation and Combustion in Non-stationary Turbulent Sprays, PhD, Chalmers University of Technology, Gothenburg, 1995.

[16] V. Sabelnikov, C. Fureby, Combust. Flame, 160 (2013) 83-96.

[17] M. Berglund, E. Fedina, C. Fureby, J. Tegnér, V. Sabel'nikov, AIAA J., 48 (2010) 540-550.

[18] C. Fureby, K. Nordin-Bates, K. Petterson, A. Bresson, V. Sabelnikov, Proc. Combust. Inst., 35 (2015) 2127-2135.

[19] M.H. Baba-Ahmadi, G. Tabor, Comput. Fluids, 38 (2009) 1299-1311.

[20] X. Li, W. Yao, X. Fan, AIAA J., 54 (2016) 3191-3211.

[21] W. Yao, Y. Yuan, X. Li, J. Wang, X. Fan, AIAA Paper 2017-2190(2017).

[22] M.P. Burke, M. Chaos, Y. Ju, F.L. Dryer, S.J. Klippenstein, Int. J. Chem. Kinet., 44 (2011) 444-474.

[23] A.S. Potturi, J.R. Edwards, AIAA J., 52 (2014) 1417-1429.

[24] F. Génin, S. Menon, AIAA J., 48 (2010) 526-539.

[25] C. Fureby, E. Fedina, J. Tegnér, Shock Waves, 24 (2014) 41-50.

[26] P. Boivin, A. Dauptain, C. Jiménez, B. Cuenot, Combust. Flame, 159 (2012) 1779-1790.

[27] T. Zhang, J. Wang, L. Qi, X. Fan, P. Zhang, J. Propul. Power, 30 (2014) 1161-1166.

[28] V.D. Poinsot T, Theoretical and numerical combustion, RT Edwards, Inc., Philadephia, USA, 2005, p.85.

List of Figure captions (Color figures in electronic version only)

Fig. 10. Schematic of the DLR combustor (unit in mm).

Fig. 2. Time-averaged profiles of streamwise velocity, streamsise velocity fluctuation, and temperature at streamwise locations.

Fig. 3. Representative case of attached flame stabilization mode with $T_0 = 607$ K and $\phi_{overall} = 0.034$: (a) instantaneous Y_{OH}, (b) instantaneous mixture reactivity and (c) instantaneous heat release rate.

Fig. 4. Distribution of λ, Y_{OH} and $\mathrm{d}\widehat{\mathrm{Q}}$ in Mach number space with $T_0 = 607$ K and $\phi_{overall}$ equals to (a) 0.022, (b) 0.034, and (c) 0.058.

Fig. 5. Lifted flame stabilization mode with $T_0 = 1784$ K and $\phi_{overall} = 0.058$: (a) instantaneous Y_{OH}, (b) instantaneous mixture reactivity and (c) instantaneous heat release rate.

Fig. 6. Scatter points' distribution in mixture fraction space for attached flame stabilization mode at $T_0 = 607$ K and lifted flame stabilization mode at $T_0 = 1784$ K.

Fig. 7. Distribution of λ, Y_{OH} and $\mathrm{d}\widehat{\mathrm{Q}}$ in Mach number space with (a) $T_0 = 1696$ K, (b) $T_0 = 1784$ K, and (c) $T_0 = 2141$ K.

Fig. 8. Dependence of the flame lifted length on T_0 for the strut-based lifted flame stabilization mode.

Fig. 9. Regime nomogram for the DLR flame stabilization.

Supplemental Material

File (1/1)	Content
Supplemental Material.docx	1. Experimental parameters of the baseline case (Table S1). 2. Parametric study on overall equivalence ratio (Table S2). 3. Parametric study on inflow stagnation temperature (Table S3). 4. Fuel injection scheme used in the 2D simulation (Fig. S1). 5. Grid convergence study for wall pressure and streamwise velocity (Fig. S2-S3). 6. 2D model validation for lifted flame stabilization mode (Fig. S4-S5). 7. Representative case of the attached flame stabilization mode (Fig. S6). 8. Effect of $\phi_{overall}$ on the attached flame stabilization mode (Fig. S7-S9). 9. Representative case of the lifted flame stabilization mode (Fig. S10). 10. Effect of $\phi_{overall}$ on the lifted flame stabilization mode (Fig. S11-S14).

Computational realization of multiple flame stabilization modes in DLR strut-injection hydrogen supersonic combustor

Kun Wu[1,2,3], Peng Zhang[2,*], Wei Yao[1,3,*] and Xuejun Fan[1,3]

1. *State Key Laboratory of High Temperature Gas Dynamics, Chinese Academy of Sciences, Beijing, 100190, People's Republic of China*
2. *Department of Mechanical Engineering, the Hong Kong Polytechnic University, Hong Kong*
3. *School of Engineering Sciences, University of Chinese Academy of Sciences, Beijing 100049, People's Republic of China*

Corresponding Author:
Peng Zhang*
Department of Mechanical Engineering, The Hong Kong Polytechnic University, Hung Hom, Hong Kong
E-mail address: pengzhang.zhang@polyu.edu.hk (P. Zhang)
Wei Yao*
Institute of Mechanics, Chinese Academy of Sciences, No. 15 Beisihuanxi Road Beijing, China
E-mail address: yaowei@imech.ac.cn (W.Yao)

Colloquium:
Detonations, Explosions and Supersonic combustion

Word Count (Method1):

The total word count (exclusive of title page, abstract) is: **6140** words (6200 required for the revision)

Word Count (was performed from automatic counting function in MS Word plus Figures/Table/References)

Abstract: 192 words, not included in word count.

Main text: 3813 words

Equations: 0 words (0 Equations, single column)

References: 524 words (28 references)

Figures: 1611 (9 figures with captions, color figures in electronic version only)

Figure	Column	Word Count
1	Single	90
2	Double	292
3	Single	162
4	Single	187
5	Single	160
6	Double	272
7	Single	189
8	Single	132
9	Single	127

Total: 6140 words

One Supplemental Material is available.

Computational realization of multiple flame stabilization modes in DLR strut-injection hydrogen supersonic combustor

Kun Wu[1,2,3], Peng Zhang[2,*] ,Wei Yao[1,3,*] and Xuejun Fan[1,3]

1. *State Key Laboratory of High Temperature Gas Dynamics, Chinese Academy of Sciences, Beijing, 100190, People's Republic of China*
2. *Department of Mechanical Engineering, the Hong Kong Polytechnic University, Hong Kong*
3. *School of Engineering Sciences, University of Chinese Academy of Sciences, Beijing 100049, People's Republic of China*

Abstract: Inspired by the existence of multiple flame stabilization modes in cavity-assisted supersonic combustor, multiple flame stabilization modes of DLR hydrogen-fueled strut injection supersonic combustor were numerically realized and analyzed for a wide ranges of inflow stagnation temperature from 607 to 2141 K and overall equivalence ratio from 0.022 to 0.110. Finite-rate chemistry large eddy simulation with detailed hydrogen mechanism was employed to capture unsteady flow characteristics and the effects of chemical kinetics. Two typical flame stabilization modes were identified and presented in a regime nomogram, which shows the dominant influence of the stagnation temperature and the secondary influence of overall equivalence ratio. At relatively low stagnation temperatures, the flame is stabilized in an "attached flame" mode, which requires a low-speed recirculation zone behind the strut for radical production and a high-speed intense combustion zone for heat release. At relatively high stagnation temperatures, the flame is stabilized in a "lifted flame" mode, in which the effect of the low-speed recirculation zone is negligible, rendering most reactions take place in supersonic flow. At intermediate stagnation temperatures, blow-out was always observed and flame cannot be stabilized in the combustor even with initially forced ignition.

Keywords: Supersonic combustion; Flame stabilization mode; DLR Strut injection scheme; Stagnation Temperature; Overall equivalence ratio.

[*] Corresponding Author: pengzhang.zhang@polyu.edu.hk (P. Zhang) and yaowei@imech.ac.cn (W. Yao)

1. Introduction

Although scramjets have shown their great potential in air-breathing propulsion at high flight Mach numbers [1], many technical problems remain unsolved. One of the problems is the flame stabilization in scramjet with moderate flight Mach numbers of 3~4, where the intake flow temperature is insufficiently high for subsequent auto-ignition after initial forced ignition and therefore additional flame-holding device is required. Wall injection [2], ramp [3], cavity [4] and strut [5] are widely-used flame-holding devices to generate low-speed flow regions where the local Damköhler numbers are effectively increased to enforce flame stabilization.

The flame stabilization mode of cavity flame holder in a dual-mode combustor fueled by both hydrogen and hydrogen/ethylene mixture was experimentally studied by Micak and Driscoll [6]. They found that the flame is stabilized either in the cavity shear layer at relatively low inflow stagnation temperature (T_0) or in the fuel jet-wake at higher T_0, and that combustion oscillates between two modes for intermediate T_0. By employing CH* chemiluminescence to diagnose an ethylene-fueled supersonic combustor with T_0 between 1200 K to 1800 K, Yuan et al. [7] recently identified three flame stabilization modes: (I) weak combustion inside the cavity or in the cavity shear layer, (II) combustion in the jet-wake, and (III) combustion oscillation between modes I and II.

Despite that these experiments are evidently different in combustor geometry, fuel injection location and fuel reactivity, the flame stabilization modes seem to be unified and the underlying physics can be understood as follows. At relatively low T_0, the chemical reactions are extremely slow in the main stream and the cavity facilitates combustion by prolonging the flow residence and fuel/oxidizer mixing times, rendering a local region of large Damköhler numbers. The cavity plays an indispensable role in providing hot spots and radicals so that the reaction zone can reside either in cavity or in the cavity shear layer (mode I).

Increasing T_0, the chemical reaction rates are increased exponentially to mitigate the reliance of the stabilized combustion on the low-speed cavity flow. As a result, reactants can be mixed and auto-ignited over a certain streamwise distance in the fuel jet-wake (mode II). Yuan et al. [8] hypothesized that the formation of aerodynamic throat near the fuel injection is germane to the observation of mode III for intermediate T_0.

Is the occurrence of these flame stabilization modes unique for cavity-based supersonic combustor? Can we observe them in strut-based supersonic combustor by varying T_0 or fuel injection? Bearing these questions in mind, we noted that a strut-injection hydrogen supersonic combustor was established by Institute of Chemical Propulsion of the German Aerospace Center (referrer to DLR combustor [9], hereinafter). The DLR experiments have been widely used for validating various numerical methods and codes, but only a few studies concern about its flame stabilization mode. Huang et al. [10] reported in their LES study that the wall-reflected oblique shock induces combustion in the subsonic bubble after the strut. Gong et al. [11] regarded the oscillation of the recirculation zones as the dominating mechanism for flame stabilization. Recently, Wu et al. [12] proposed a three-stage flame stabilization mechanism based on the analysis of generation, transportation and consumption of radicals. Regardless of the different explanations, the DLR combustion is agreed to be categorized to mode I in which the flame is attached to the fuel injection strut. This is because the relatively low T_0 hinders auto-ignition, and the combustion behind the strut, which plays the same role as cavity in creating a low-speed recirculation zone, is necessary to sustain combustion in the downstream.

Because of the fixed T_0 (607 K) and fuel injection, the DLR supersonic combustion experiment does not show any evidence for mode II or III. Qin et al. [13] carried out a LES study on the DLR combustor with three different T_0 of 460K, 568 K and 960 K, but with fixed Mach number and global equivalence ratio. They found that, the stabilized flames at

460 K and 568 K are similar to modes I but the combustion eventually dies out at 960K after initial forced ignition. Therefore, the problems still remain unsolved that whether mode II and III can exist for the DLR combustor and that what is the underlying physics in terms of flow-chemistry interaction. The present study aims to computationally reproduce and characterize main features of these different flame stabilization modes in strut-injection DLR combustor.

2. Computational Specifications

2.1 Numerical methods and physical models

The numerical methods and physical models adopted by the present study have been expatiated in great detail and sufficiently validated in [12]. As a brief summary, the spatially filtered equations for three-dimensional, compressible, multicomponent, reacting flow are solved. The ideal gas mixture is assumed to be linear viscous fluid abiding Fourier heat conduction and Fickian diffusion; the viscosity is calculated by Sutherland's law; thermal conductivities and mass diffusivities are obtained from viscosity by assuming constant Prandtl number ($Pr = 0.7$) and Schmidt number ($Sc = 0.7$). The subgrid turbulence terms are closed by employing the one-equation kinetic energy model [14]. Turbulent Prandtl number, Pr_{t}, and Schmidt number, Sc_{t}, are set to 0.72 and 0.9, respectively. The filtered reaction rates are modeled using the partially stirred reactor (PaSR) model [15], which and its variation [16] have been extensively used in the studies of self-ignition [17] and supersonic combustion [18].

A density-based flow solver, astroFoam, which was developed based on the OpenFoam platform, was adopted in the study. The convective fluxes at faces are constructed using a second-order TVD (Total Variation Diminishing) scheme. The time-integration is marched by the second-order Crank-Nicholson scheme [19]. This code has been extensively validated for non-reactive highly underexpanded jet [20] and supersonic combustion [21].

2.2 Computational setups

The DLR combustor [9] is schematized in Fig. 1. Coordinates in both x and y directions are normalized to $\hat{x}$ and $\hat{y}$ using combustor's characteristic length L and height H. Ma=2.0 vitiated air was supplied through a rectangular-shaped entrance of 50 mm in height and 40 mm in width. The combustor upper wall diverges slightly by 3º from $\hat{x} = -0.039$ to compensate the growing boundary layer. Hydrogen was sonically injected from an array of 15 evenly-spaced injectors on the base of a wedge-shape strut. The strut is 32 mm in length and 6º in half divergence angle and installed along the combustor center line. The fuel orifices at $\hat{x} = 0$ are 1.0 mm in diameter and their adjacent distance is 2.4 mm in the z-direction.

In the DLR experiment, the air stagnation pressure and temperature are 0.78 MPa and 607 K. The vitiated air was composed by oxygen of 23.2%, nitrogen of 73.6% and vapor water of 3.2% in mass. The fuel stagnation pressure and temperature are 0.189 MPa and 288 K; the overall equivalence ratio is $\phi_{overall} = 0.034$. For the present computational study, the inflow stagnation temperature (T_0) varies over a wide range from 607 K to 2141 K and $\phi_{overall}$ varies significantly from 0.022 to 0.110. To facilitate the following discussion, velocity, temperature and heat release rate are presented in dimensionless form of $\hat{u}_i = u_i/U_\infty^{air}$, $\hat{T} = T/T_\infty^{air}$, $d\hat{Q} = dQ/C_pT$, and $\hat{T}_0 = T_0/T_0^{exp}$.

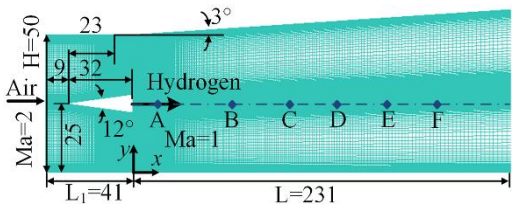

Fig. 1. Schematic of the DLR combustor (unit in mm).

The present work adopts the 2D computational model proposed by Wu et al. [12]. In the 2D model shown in the Support Materials (Fig. S1), the fuel orifice is replaced by a 2D slot-like injector with a periodic injection scheme to keep $\phi_{overall}$ the same as in the experiment and meanwhile retains the local flow structures in the vicinity of the strut. The applicability

of the 2D model in capturing the spatial distributions of pressure, velocity, and temperature was fully validated, and its uncertainty in resolving the near-field turbulent wake structures was also recognized [12]. It should be emphasized that the 2D model can remarkably reduce the computational cost, particularly when the computation is integrated with the Burke et al.'s [22] detailed hydrogen oxidation mechanism consisting of 9 species and 19 reactions, to enable the systematic study of flame stabilization and the result analysis from the perspective of chemical kinetics.

Block-structured hexahedral grids were used with clustering applied at the strut shear layer and wake region. The average and maximum of the grid resolution in the mixing region are 0.08 mm and 0.15 mm, respectively. They are smaller than 0.25 mm (in average) in the hybrid LES/RANS study of Potturi and Edwards [23] and 1.0 mm (in average) in the LES study of Génin and Menon [24]. The comprehensive grid convergence study based on three sets of grid (0.19, 0.27 and 0.52 Million) has been presented in [12] and further study in the Supporting Materials (Fig. S2-S3). Dirichlet boundary conditions are used for all variables at the air and fuel inlet except for velocity. The velocity profile at the inflows is specified as a superposition of their mean values and sinusoidal perturbation with 5% of their amplitude of the mean values. At the combustor outlet, all variables are extrapolated from the interior. At the combustor and strut walls, no-slip boundary condition is used for velocity while zero gradient conditions are used for all other variables. The physical time step is set to 3.5×10^{-9} s which corresponds to a maximum Courant-Friedrich-Lewy number of 0.4. The simulations were run for about 14 flow-through times ($t_f = L/U_\infty \approx 3 \times 10^{-4}$ s), where $7t_f$ was used to ensure statistical steady state while the remainder to collect statistical data.

3. Results and Discussion

3.1 Numerical validation

The present 2D model has been validated in [12] against the DLR experiment [9], and compared with Potturi et al.'s [23] simulation results. To further examine its uncertainty in predicting turbulent flow, the LES results of Fureby et al. [25] on the full-scale DLR combustor including all fifteen fuel injectors are presented in Fig. 2 for comparison. The streamwise locations are annotated in Fig.1 where $\hat{x}_A = 0.048$, $\hat{x}_B = 0.251$, $\hat{x}_C = 0.390$, $\hat{x}_D = 0.498$, $\hat{x}_E = 0.606$ and $\hat{x}_F = 0.719$.

The DLR experiment reported the measurement of streamwise velocity at locations A, B and E, as shown in Fig. 2(a)-(c). At location A, the 2D model overpredicts the streamwise velocity, probably attributable to its uncertainty in resolving the three-dimensional flow structure in the near field around the strut rear. Qualitative discrepancies can be found between Fureby et al.'s prediction and the experimental data. At location B, the predicted velocity profile, albeit narrow in width, agrees well with the trend of the experimental data. At location E, the present result shows very good agreement with the experimental data, but Fureby et al.'s results however show an opposite trend. The comparison with 3D simulation has been elaborated in Ref [12]. Although the present 2D model may result in the single temperature peak due to the relative deficiency in fully capturing the 3D flow characteristics in the vicinity of the strut, it produces good predictions in all the downstream locations.

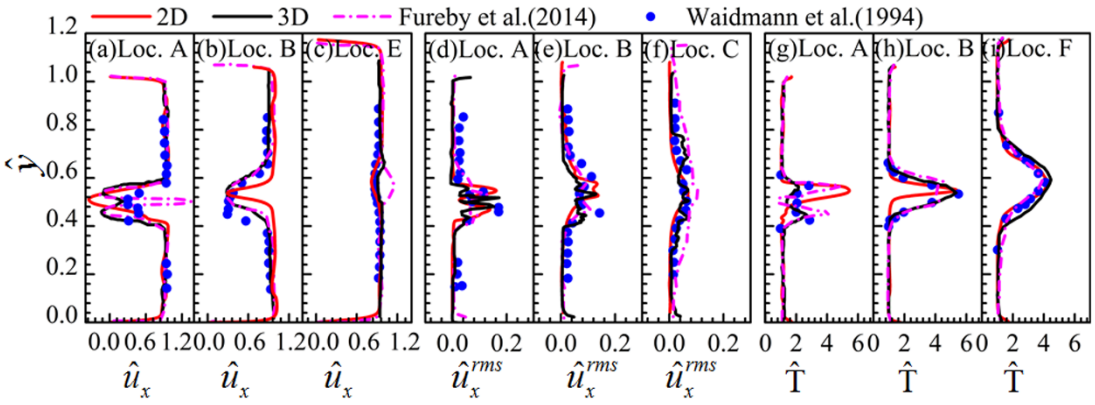

Fig. 2. Time-averaged profiles of streamwise velocity, streamsise velocity fluctuation, and temperature at streamwise locations.

The experimental fluctuation velocity profiles are available at locations A, B and C, as shown in Fig. 2(d)-(f). The present results show very good agreement with experimental data, indicating that the 2D model can well capture the unsteadiness of the streamwise flow that dominates the DLR flow. Fureby et al.'s results slightly overshoot the experimental data at location C. Fig. 2(g)-(i) show the time-averaged temperature profiles at location A, B, and F. It can be seen that the both simulated temperature profiles do not reproduce the two temperature peaks at location A, while they achieve satisfactory good agreement at the downstream locations B and F. Due to the lack of experimental data at higher T_0, the present 2D model was further validated against 3D simulation for T_0=2141 K, the highest T_0 considered in the study. These results are shown in the Supporting Materials (Fig. S4-S5) and further validate the 2D model at high T_0.

3.2 Attached flame stabilization mode

A representative (original experimental) case of the attached flame stabilization mode is shown in Fig. 3, where $T_0 = 607$ K and $\phi_{overall} = 0.034$. As has been thoroughly analyzed in [12], the entire combustion process can be divided into three stages along the streamwise direction, such as the induction stage where ignition occurs and active radicals are produced, the transitional stage through which radicals are advected to the downstream, and the intense combustion stage where most heat release occurs. From the mass fraction of OH radicals, as shown in Fig. 3(a), the three-stage combustion stabilization mode can be clearly observed, indicating the radical production, transportation and consumption are essential in attached flame stabilization mode. Moreover, the time-averaged result, as seen in Fig. S6 in the Supporting Materials, also shows similar characteristics and further substantiates the assertion of the three-staged flame stabilization mode.

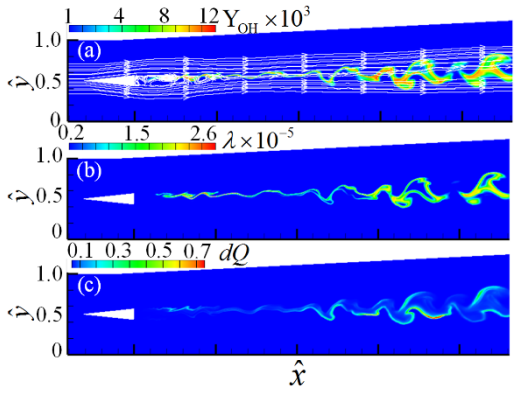

Fig. 3. Representative case of attached flame stabilization mode with $T_0 = 607$ K and $\phi_{overall} = 0.034$: (a) instantaneous Y_{OH}, (b) instantaneous mixture reactivity and (c) instantaneous heat release rate.

By comparing hydrogen oxidation mechanisms at various different levels of reduction, the controlling reaction steps were identified by Wu et al. [12] to be the two chain branching reactions (R1) $H+O_2 \rightarrow O+OH$ and (R2) $O+H_2 \rightarrow H+OH$, both of which produce OH radicals, and (R3) $H_2+OH \rightarrow H+H_2O$, which consumes OH radicals and releases heat. To quantitatively measure the competition among these reaction steps, we adopted the mixture reactivity, λ, defined by Boivin et al. [26] as $\lambda = 2k_1c_{O_2}\left[(1+2B)^{1/2}-1\right]/B$, where $B = 4k_1c_{O_2}(k_1c_{O_2}+k_2c_{H_2}+k_3c_{H_2})/k_2k_3c_{H_2}^2$. k_1, k_2 and k_3 are the rate constants of R1, R2 and R3, and c the molar concentration of species. According to the definition, the mixture reactivity index λ is inversely proportional to the auto-ignition delay time under homogeneous conditions. Consequently, a large value of λ means that reaction R1 and R2 control the reactivity of the mixture and facilitate ignition. For small λ, reaction R3 dominantly consumes OH radicals and therefore retards ignition.

Figure 4 shows λ, Y_{OH}, and $d\hat{Q}$ in a Mach number space. The evident concentration of λ and Y_{OH} in the subsonic regime reemphasizes the important role of the low-speed recirculation zone behind the strut in producing active radicals. In contrast, $d\hat{Q}$ is distributed over the whole Mach number range, indicating that both the recirculation zone and the downstream intense combustion zone are responsible for the heat release.

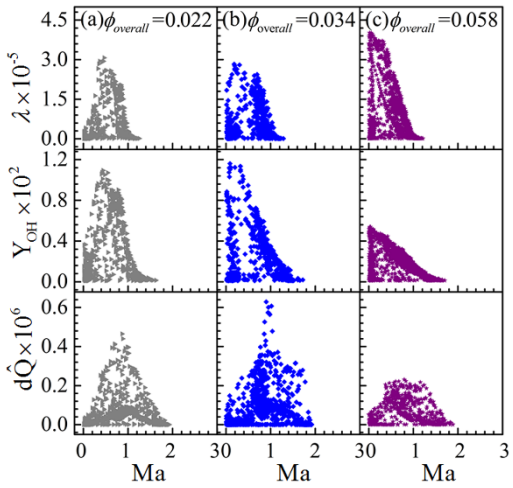

Fig. 4. Distribution of λ, Y_{OH} and $d\hat{Q}$ in Mach number space with $T_0 = 607$ K and $\phi_{overall}$ equals to (a) 0.022, (b) 0.034, and (c) 0.058.

With decreasing $\phi_{overall}$ to 0.022, as shown in Fig. 4(a), peak values of λ and Y_{OH} tend to shift to higher subsonic regime. This can be understood that, because of the reduced total heat release at the smaller $\phi_{overall}$, the thermal expansion of the reaction zone becomes smaller as shown in Fig. S7(a)-S9(a) in the Supporting Material. Therefore, the influence of the reaction zone on the main stream is reduced. With increasing $\phi_{overall}$ to 0.058, more heat release and the wider reaction zone can be seen, as shown in Fig. S7(c)-S9(c) in the Support Material. This in turn decelerates the main stream so that the combustion in the strut wake is intensified. This tendency can be seen in Fig. 4(c) where the reaction zones show subsonic-shifting and the peak values of λ and Y_{OH} move to smaller Ma. Regardless of these changes, the main feature of the attached flame stabilization mode is retained. Furthermore, the backpressure caused by the increased heat release in the present case is insufficient to alter the combustor inflow condition. Therefore, the combustor unstart observed by Zhang et al. [27] in cavity flame-holding supersonic combustor by increasing fuel injection was not observed in the present study.

3.3 Lifted flame stabilization mode

Fig. 5 shows the case with $T_0 = 1784$ K and $\phi_{overall} = 0.058$. The low-speed recirculation zone indicated by the converging streamlines behind the strut is suppressed by the main flow to a very small region, where Y_{OH} is negligibly small. The distribution of λ is similar to that of Y_{OH} and again indicates that R1-R3 are all suppressed in the strut wake flow. The little reliance of the flame stabilization on the local recirculation zone and the far downstream location of the lifted flame suggest that the present stabilization model resembles the fuel jet wake in the cavity-based supersonic combustion experiment [6]. Furthermore, the time-averaged result, as shown in Fig. S10 in the Supporting Materials, also resembles similar lifted flame stabilization characteristics. It is noted that the present fuel injection is made on the base of the strut so that the jet wake is in the downstream of the strut. In the cavity-based supersonic combustor [7, 8], a cross-flow of fuel was injected to the upstream of the cavity and the jet wave is above the cavity.

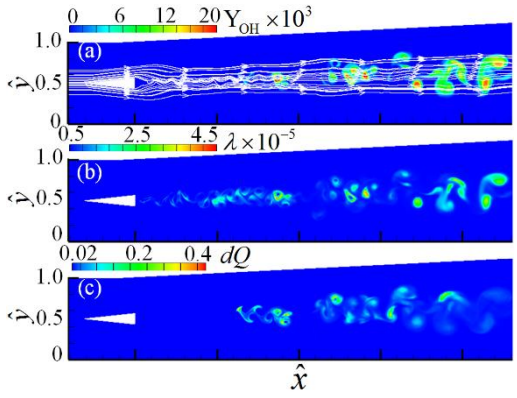

Fig. 5. Lifted flame stabilization mode with $T_0 = 1784$ K and $\phi_{overall} = 0.058$: (a) instantaneous Y_{OH}, (b) instantaneous mixture reactivity and (c) instantaneous heat release rate.

To further reveal the difference between two flame stabilization modes, plots of Y_{OH}, λ, $d\hat{Q}$ in the mixture fraction space are presented in Fig. 6. The mixture fraction (denoted by Z) refers to the conventional definition [28] as $Z = (\upsilon Y_F - Y_{O2} + Y_{O2,2})/(\upsilon Y_{F,1} + Y_{O2,2})$ in which υ is the stoichiometric oxygen-to-fuel mass ratio. In the strut shear layer and wake flow near the fuel injection, the mixture ranges from fuel rich to nearly stoichiometric rendering $Z \geq Z_{st}$. As the result of the mixing between the fuel jet and main air flow, Z

gradually decreases in the downstream. For the attached flame mode at $T_0 = 607$ K, most OH appears around Z_{st}, implying that it forms in the recirculation zone with long flow residence time for mixing. Similar trend can be found for λ since it represents the competition among reaction R1-R3 for OH radicals. For the lifted flame mode at $T_0 = 1784$ K, most OH appears at $Z<Z_{st}$, implying that it is not formed in the "fuel-rich" recirculation zone but in the "fuel-lean" far downstream.

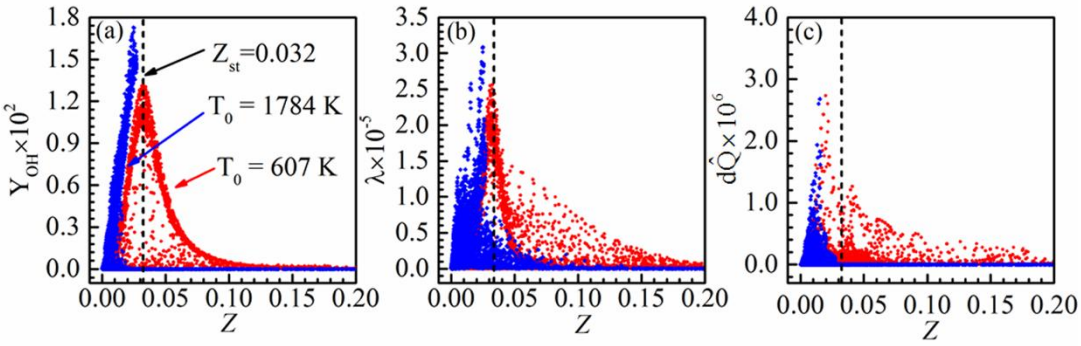

Fig. 6. Scatter points' distribution in mixture fraction space for attached flame stabilization mode at $T_0 = 607$ K and lifted flame stabilization mode at $T_0 = 1784$ K.

Fig. 7 shows λ, Y_{OH}, and $d\hat{Q}$ in Mach number space for various T_0. Regarding Y_{OH} and $d\hat{Q}$, the most prominent feature of the lifted flame mode is the transition of the primary combustion zone to the supersonic regime, compared with that in Fig. 4. It is also found that the lifted flame at $T_0 = 1696$ K moves to farther downstream and significantly decreased radical formation and heat release occur in the supersonic regime, indicating the increasing tendency of the flame blow-out with decreasing T_0.

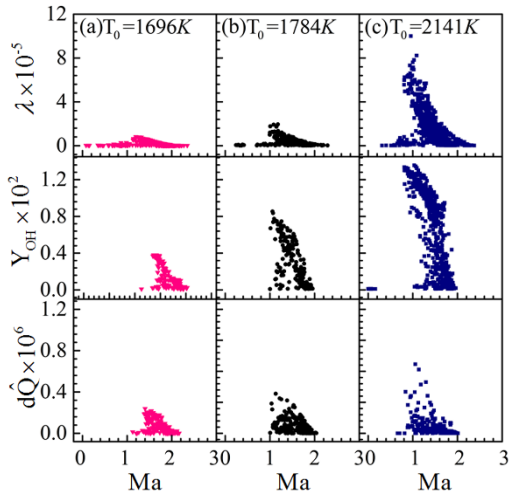

Fig. 7. Distribution of λ, Y_{OH} and $\mathrm{d}\hat{\mathrm{Q}}$ in Mach number space with (a) $T_0 = 1696$ K, (b) $T_0 = 1784$ K, and (c) $T_0 = 2141$ K.

It is rather interesting to investigate the flame lift-off distance as an indicator of flame blowout trend. By following the definition introduced by Micka and Driscoll [6], an iso-line characterizing the reaction zone border was defined in instantaneous OH contour with prescribed threshold value, i.e., $Y_{OH}(Threshold) = 10^{-5}$. The most upstream axial locations of a series of temporal snapshots were calculated then averaged to get the final statistical result as shown in Fig. 8. To verify that the flame lift-off distance is insensitive to the threshold, two different thresholds by an order of magnitude were used and both show the consistent tendency as follows. In the present problem with a fixed Mach number, higher T_0 means higher static temperature T and speed of sound ($c \sim \sqrt{T}$), which tends to push the flame further downstream. In the meantime, the increased temperature will exponentially increase chemical reaction rates [$\sim \exp(-E_a/RT)$], rendering the intense combustion in higher velocity flow possible. This explains the lift-off distance in the lifted flame stabilization mode decreases with T_0.

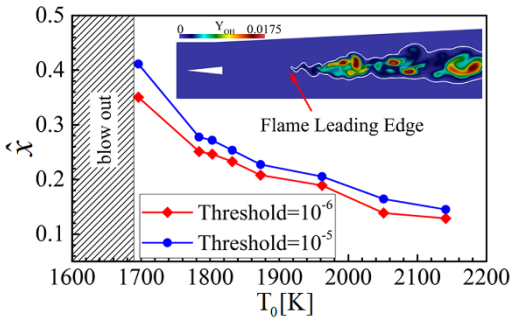

Fig. 8. Dependence of the flame lifted length on T_0 for the strut-based lifted flame stabilization mode.

3.4 Regime nomogram for strut-based flame stabilization

To systematically quantify the influence of T_0 and $\phi_{overall}$ on the flame stabilization, we studied 21 cases with T_0 varies from 607 K to 2141 K and $\phi_{overall}$ from 0.022 to 0.110. Details of all the cases are listed in Table S2-S3 in the Supporting Material. It is noted that the variation of T_0 with the fixed Mach number slightly changes the air flow rate and thus the overall equivalence ratio by 13% in maximum, which does not cause qualitative difference to the flame stabilization modes, as has been substantiated above.

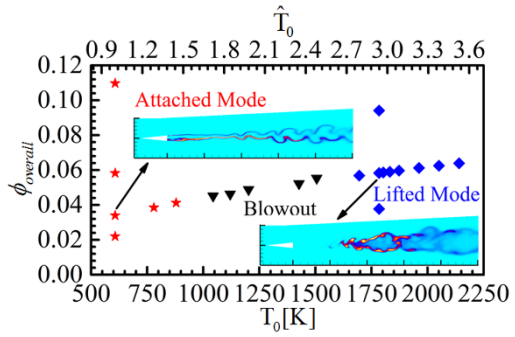

Fig. 9. Regime nomogram for the DLR flame stabilization.

The identified flame stabilization modes are depicted in Fig. 9 as a regime nomogram in the $T_0 - \phi_{overall}$ space. Under relatively low T_0, the flame in the DLR combustor stabilizes in attached mode while $T_0 \geq 1696$ K the flame can again be stabilized however in another distinct mode. It is also seen that the variation of $\phi_{overall}$ in the range concerned does not cause transition between attached and lifted flame stabilization modes, indicating that overall

equivalence ratio is a secondary factor in determining flame stabilization mode in the DLR combustor. The influence of $\phi_{overall}$ on the combustion characteristics is shown in Fig. S11-S14 in Supporting Material.

In the intermediate temperature range of $1044 < T_0 < 1696$ K, the flame cannot be stabilized even being forced ignited initially. This has been confirmed by our repeated simulation runs by using different initial conditions and ignition methods. In fact, at the fixed inflow Mach number, the inflow velocity increases with T_0 and causes more heat loss from the combustion zone to the main air flow, therefore tending to destabilize the flame. This can be used to explain why combustion oscillation, which was hypothesized to occur in this temperature range, was not observed in the present simulation. As elaborated in the introduction, the formation of aerodynamic throat is essential for oscillation flame stabilization mode but the combustion in DLR configuration is unable to provide sufficient heat release to thermally chock the combustor. Therefore, the oscillation between the two modes could not be realized in the present study. A possible solution to the problem is to modify the geometry of the DLR combustor to increase the possibility of thermal chocking. This hypothesis merits future investigations.

4. Concluding Remarks

In the present study, flame stabilization modes in a hydrogen-fueled strut injection DLR supersonic combustor were systematically investigated employing finite-rate chemistry large-eddy simulation with detailed hydrogen mechanism of Burke et al. [22] . Two different flame stabilization modes were identified by multiple metrics such as flow field visualization, radical evolution, and heat release, in both Mach number and mixture fraction spaces.

For the attached flame stabilization mode occurring at relatively low T_0 (607 to 879 K), the entire combustion process can be divided into three stages, such as the induction stage where ignition occurs and active radicals are produced, the transitional stage through which radicals are advected to the downstream, and the intense combustion stage where most heat release occurs. The low-speed recirculation zone behind the strut is indispensable to the combustion stabilization by producing active radicals.

For the lifted flame stabilization mode occurring at relatively high T_0 (1696 to 2141 K), a lifted flame is manifest and the effect of the low-speed recirculation zone behind the strut becomes negligible. Furthermore, the flame lifted distance deceases with increasing T_0 because the exponentially increased reaction rates shorten the distance between the fuel injection and the autoignition. In contrast to that the main combustion zones of the attached flame mode resides in subsonic regions, the main combustion zone in the lifted flame mode is in the supersonic region.

The present parametric study shows that significant variation in the overall equivalence does not cause the change of stabilization mode. In the intermediate range of T_0 (1044 to 1506 K), the hypothesized combustion oscillation was not observed and the initially forced ignition always results in eventual blowout. The existence of combustion oscillation mode in the DLR supersonic combustor remains an unsolved problem.

Acknowledgements

The work at Chinese Academy of Sciences was supported by Training Program of the Major Research Plan of the National Natural Science Foundation of China (Grant No. 91641110) and National Natural Science Foundation of China (Grant No. 11502270). The

work at the Hong Kong Polytechnic University was supported partly by RGC/GRF (PolyU 152217/14E, PolyU 152651/16E) and partly by NSFC (No. 91641105).

References

[1] J.J. Bertin, R.M. Cummings, Prog. Aerosp. Sci., 39 (2003) 511-536.

[2] W. Xianyu, L. Xiaoshan, D. Meng, L. Weidong, W. Zhenguo, Chin. J. Aeronaut., 20 (2007) 488-494.

[3] J.M. Donohue, J.C. McDaniel, H. Haj-Hariri, AIAA J., 32 (1994) 1860-1867.

[4] F.W. Barnes, C. Segal, Prog. Aerosp. Sci., 76 (2015) 24-41.

[5] K.Y. Hsu, C.D. Carter, M.R. Gruber, T. Barhorst, S. Smith, J. Propul. Power, 26 (2010) 1237-1246.

[6] D.J. Micka, J.F. Driscoll, Proc. Combust. Inst., 32 (2009) 2397-2404.

[7] Y. Yuan, T. Zhang, W. Yao, X. Fan, P. Zhang, Proc. Combust. Inst., 36 (2017) 2919-2925.

[8] Y. Yuan, T. Zhang, W. Yao, X. Fan, J. Propul. Power, 31 (2015) 1524-1531.

[9] W. Waidmann, F. Alff, M. Böhm, U. Brummund, W. Clauß, M. Oschwald, Space Technol., 15 (1994) 421-429.

[10] Z.-w. Huang, G.-q. He, F. Qin, X.-g. Wei, Int. J. Hydrogen Energy, 40 (2015) 9815-9824.

[11] C. Gong, M. Jangi, X.-S. Bai, J.-H. Liang, M.-B. Sun, Int. J. Hydrogen Energy, 42 (2017) 1264-1275.

[12] K. Wu, P. Zhang, W. Yao, X. Fan, Combust. Sci. Technol., 189 (2017) 2154-2179.

[13] F. Qin, Z.-w. Huang, G.-q. He, S. Wang, X.-g. Wei, B. Liu, Int. J. Hydrogen Energy, 42 (2017) 21360-21370.

[14] A. Yoshizawa, Phys. Fluids, 29 (1986) 2152-2164.

[15] A. Karlsson, Modeling Auto-ignition, Flame Propagation and Combustion in Non-stationary Turbulent Sprays, PhD, Chalmers University of Technology, Gothenburg, 1995.

[16] V. Sabelnikov, C. Fureby, Combust. Flame, 160 (2013) 83-96.

[17] M. Berglund, E. Fedina, C. Fureby, J. Tegnér, V. Sabel'nikov, AIAA J., 48 (2010) 540-550.

[18] C. Fureby, K. Nordin-Bates, K. Petterson, A. Bresson, V. Sabelnikov, Proc. Combust. Inst., 35 (2015) 2127-2135.

[19] M.H. Baba-Ahmadi, G. Tabor, Comput. Fluids, 38 (2009) 1299-1311.

[20] X. Li, W. Yao, X. Fan, AIAA J., 54 (2016) 3191-3211.

[21] W. Yao, Y. Yuan, X. Li, J. Wang, X. Fan, AIAA Paper 2017-2190(2017).

[22] M.P. Burke, M. Chaos, Y. Ju, F.L. Dryer, S.J. Klippenstein, Int. J. Chem. Kinet., 44 (2011) 444-474.

[23] A.S. Potturi, J.R. Edwards, AIAA J., 52 (2014) 1417-1429.

[24] F. Génin, S. Menon, AIAA J., 48 (2010) 526-539.

[25] C. Fureby, E. Fedina, J. Tegnér, Shock Waves, 24 (2014) 41-50.

[26] P. Boivin, A. Dauptain, C. Jiménez, B. Cuenot, Combust. Flame, 159 (2012) 1779-1790.

[27] T. Zhang, J. Wang, L. Qi, X. Fan, P. Zhang, J. Propul. Power, 30 (2014) 1161-1166.

[28] V.D. Poinsot T, Theoretical and numerical combustion, RT Edwards, Inc., Philadephia, USA, 2005, p.85.

List of Figure captions (Color figures in electronic version only)

Fig. 10. Schematic of the DLR combustor (unit in mm).

Fig. 2. Time-averaged profiles of streamwise velocity, streamsise velocity fluctuation, and temperature at streamwise locations.

Fig. 3. Representative case of attached flame stabilization mode with $T_0 = 607$ K and $\phi_{overall} = 0.034$: (a) instantaneous Y_{OH}, (b) instantaneous mixture reactivity and (c) instantaneous heat release rate.

Fig. 4. Distribution of λ, Y_{OH} and $\mathrm{d}\widehat{\mathrm{Q}}$ in Mach number space with $T_0 = 607$ K and $\phi_{overall}$ equals to (a) 0.022, (b) 0.034, and (c) 0.058.

Fig. 5. Lifted flame stabilization mode with $T_0 = 1784$ K and $\phi_{overall} = 0.058$: (a) instantaneous Y_{OH}, (b) instantaneous mixture reactivity and (c) instantaneous heat release rate.

Fig. 6. Scatter points' distribution in mixture fraction space for attached flame stabilization mode at $T_0 = 607$ K and lifted flame stabilization mode at $T_0 = 1784$ K.

Fig. 7. Distribution of λ, Y_{OH} and $\mathrm{d}\widehat{\mathrm{Q}}$ in Mach number space with (a) $T_0 = 1696$ K, (b) $T_0 = 1784$ K, and (c) $T_0 = 2141$ K.

Fig. 8. Dependence of the flame lifted length on T_0 for the strut-based lifted flame stabilization mode.

Fig. 9. Regime nomogram for the DLR flame stabilization.

Supplemental Material

File (1/1)	Content
Supplemental Material.docx	1. Experimental parameters of the baseline case (Table S1). 2. Parametric study on overall equivalence ratio (Table S2). 3. Parametric study on inflow stagnation temperature (Table S3). 4. Fuel injection scheme used in the 2D simulation (Fig. S1). 5. Grid convergence study for wall pressure and streamwise velocity (Fig. S2-S3). 6. 2D model validation for lifted flame stabilization mode (Fig. S4-S5). 7. Representative case of the attached flame stabilization mode (Fig. S6). 8. Effect of $\phi_{overall}$ on the attached flame stabilization mode (Fig. S7-S9). 9. Representative case of the lifted flame stabilization mode (Fig. S10). 10. Effect of $\phi_{overall}$ on the lifted flame stabilization mode (Fig. S11-S14).